Trajectory Approach to the Mode-Selected Photodissociation of CS_2

Huei Tarng Liou,* Yih Chung Chang, and Zeyoung Liou

Institute of Atomic and Molecular Sciences, Academia Sinica, P.O. Box 23-166, Taipei, Taiwan

Received: January 2, 2006; In Final Form: February 16, 2006

Through the study of photodissociation events in the CS_2 molecule that originate in various selected vibrational modes, but terminate in the same final predissociation state, we looked for the evidence that photodissociation processes can depend on the initial conditions. Such dependence would not occur within RRKM theory, because of its statistical assumptions. The experimental results were compared with trajectory calculations in normal mode coordinates, in which initial conditions were given in terms of coordinates and momenta. We have found that the photodissociation rate for events originating in the combination ν_1, ν_2 mode is higher than that for events from the pure ν_2 mode, and shows a large variation along the vibrational progression. The experimental observations agree with the trajectory calculations. In addition, the trajectory calculations predict that photodissociation events initiated at small values of the vibrational coordinates result in larger dissociation rates at low excess energy above the dissociation limit, while events from large values of the coordinates result in larger dissociation rates at high excess energies.

I. Introduction

A dissociation process changes a molecule from bound to unbound. As a result, the kinetic energy of the molecule nuclei can no longer be described by a rotational energy and a vibrational energy, as is done for a bound state. In the classical dynamical approximation, the total energy of the molecular nuclei can be divided into potential energy, kinetic energy, and dissipative energy. In the case of photodissociation, the absorbed photon energy $h\nu$ is at first converted into electron energy (eq 1), which is then transformed into nuclear-motion energy (eq 2). Both of these equations include an energy dissipative term.

$$T(\ddot{q}_e) + D(\dot{q}_e) + V(q_e) = E(h\nu) \tag{1}$$

$$T(\ddot{q}_n) + D(\dot{q}_n) + V(q_n) = E(\dot{q}_n, q_n) \tag{2}$$

In the case where the statistical criterion is satisfied, the excess energy is distributed statistically among all energy modes in a time that is negligible compared to the unimolecular dissociation time, the dissociation rate for the system can be predicted by RRKM[1−6] theory, and this dissociation rate is given by eq 3.

$$K(E) = \frac{(E - E^0)^{N-1}}{\rho(E)} \tag{3}$$

Equation 3 implies that, for a system satisfying the statistical criterion, the dissociation rate $K(E)$ is determined by the number of degrees of freedom N and the amount of excess energy available ($E - E^\circ$), but is independent of initial conditions such as the kinetic energy and coordinates before the dissociation, and of the dynamics during the dissociation process.

In this study, we are interested in situations where the statistical criterion is not satisfied. According to the Franck−Condon principle, we can regard the initial conditions for the molecular nuclei, such as internal coordinates and kinetic energy, as unchanged during the electron transition.[7] The molecular nuclei then readjust after the electron transition is complete. We have looked for experimental evidence that, for systems that do not satisfy the statistical criterion, the photodissociation process is dependent on the initial conditions. We have carried out a number of classical trajectory calculations to trace the effect of different initial conditions on the dissociation rate for the ground-state potential energy surface of CS_2.

For the case of a B−A−B triatomic molecule with C_{2v} symmetry, the potential energy surface in dimensionless normal mode coordinates q_i[8−11] is described by eq 4.

$$\frac{V}{hc} = \frac{1}{2}(\omega_1 q_1^2 + \omega_2 q_2^2 + \omega_3 q_3^2) + k_{111} q_1^3 + k_{122} q_1 q_2^2 + k_{133} q_1 q_3^2 + k_{1111} q_1^4 + k_{1122} q_1^2 q_2^2 + k_{1133} q_1^2 q_3^2 + k_{2222} q_2^4 + k_{2233} q_2^2 q_3^2 + k_{3333} q_3^4 + \ldots \tag{4}$$

When the motion of nuclei is represented by a classical trajectory it is of interest to know whether the potential of the initial state or that of the final state of the photoabsorption process should be specified. If the initial state were to be specified, the potential function above suggests a possible mechanism to manipulate the path of photodissociation by varying the initial conditions. For instance, by exciting the ν_1 mode, the ν_2 mode, or their combination modes to increase the interaction containing q_1 or q_2 or their combinations, the symmetric dissociation, that is $AB_2 \rightarrow A + B_2$, can be enhanced. Similarly, by exciting the ν_3 mode, the antisymmetric dissociation, that is $AB_2 \rightarrow AB + B$, can be enhanced.[12]

To investigate the dependence of the photodissociation rate on the initial conditions, we carried out experiments in which the photodissociation of CS_2 is initiated from various selected vibrational modes, but proceeds to the same final predissociation state for dissociation. At the same time, we deduced dissociation rates for comparison with the experimental results by performing trajectory calculations in normal mode coordinates, in which the initial conditions such as coordinates and momentum were given.

* Address correspondence to this author. E-mail: htliou@po.iams.sinica.edu.tw.

10.1021/jp060012s CCC: $33.50
Published on Web 03/16/2006

TABLE 1: Vibrational Constants of the $X^1\Sigma_g^+$ State of CS_2

	Liou et al.[12] (cm^{-1})
ω_1	672.276
ω_2	398.019
ω_3	1558.680

TABLE 2: Force Constants of the $X^1\Sigma_g^+$ State of CS_2

	Liou et al.[12] (cm^{-1})		Liou et al.[12] (cm^{-1})
k_{111}	−16.102	k_{1133}	7.397
k_{122}	39.378	k_{2222}	1.638
k_{133}	130.249	k_{2233}	−14.538
k_{1111}	0.310	k_{3333}	3.849
k_{1122}	−0.5066		

II. Trajectory Calculation

A. Methods. Tables 1 and 2 give the vibrational and force constants (cm^{-1}) of the $X^1\Sigma_g^+$ state of CS_2 that are used in this calculation, represented in dimensionless normal coordinates. The constants were obtained from the spectroscopic studies of Liou et al.[12−14] The resulting potential surface function reasonably describes the spectroscopic data for energies lower than 12830 cm^{-1} with an accuracy limit less than 2.3 cm^{-1}.

The form of the potential surface is described in eq 4. The classical Hamiltonian, in normal mode coordinates, takes the form:

$$H = T + V = \frac{1}{2}({p_1}^2 + {p_2}^2 + {p_3}^2) + \frac{V(q_1,q_2,q_3)}{hc} \qquad (5)$$

where p_1, p_2, and p_3 are the time derivatives of the dimensionless normal coordinates. By the classical Hamiltonian equations, we can obtain the equations of motion for the molecule in normal mode coordinates:

$$\dot{q}_i = \frac{\partial H}{\partial p_i} = p_i \qquad (6)$$

$$\dot{p}_i = \frac{\partial H}{\partial p_i} \qquad (7)$$

which can be twice numerically integrated by the 4th order Runge−Kutta integration method[15] to yield the classical trajectory in normal mode coordinates.

B. Calculations. We attempt to show, for a system with given total energy, that the initial conditions of the system at the onset of the photoexcitation, such as the amplitude of the initial vibration modes, will affect the dissociation rate of the molecule.

The initial coordinate q_3 is fixed at $\sqrt{2}$ for zero q_3 excitation. We then select a set of initial q_1, q_2 values on the potential energy surface that form a 21 × 21 point square grid in the q_1, q_2 plane. To determine the maximum and minimum q_1 and q_2 values, we arbitrarily select some value of total initial energy E_0, in this case E_0 = 1.5, 1.10, 1.15, and 1.20. The Quadrant I corner of the grid is selected so that $E_0 = (1/hc)V(q_1,q_2,q_3)$ at this point, where $(1/hc)V(q_1,q_2,q_3)$is the potential energy surface defined in eq 4. Due to the shape of the potential surface, we can know that the potential energy at all other points on the square grid will be equal to or lower than the potential energy at this point. The difference between the initial total energy E_0 and the initial potential energy $E_U = (1/hc)V(q_1,q_2,q_3)$ at each point on the grid is defined as the initial kinetic energy E_K at that particular grid point.

In this series of trajectory calculations, we place the initial kinetic energy in the q_2 vibration mode $p_2 = dq_2/dt = \sqrt{2}(E_0 - E_U)^{1/2}$. We then have a set of initial conditions $(q_1, q_2, q_3, p_1, p_2, p_3) = (q_1, q_2, \sqrt{2}, 0, p_2, 0)$ for each grid point. The system is then allowed to evolve in time from that set of initial conditions. Dissociation is said to occur when the system crosses one of the two lower saddle points.[16]

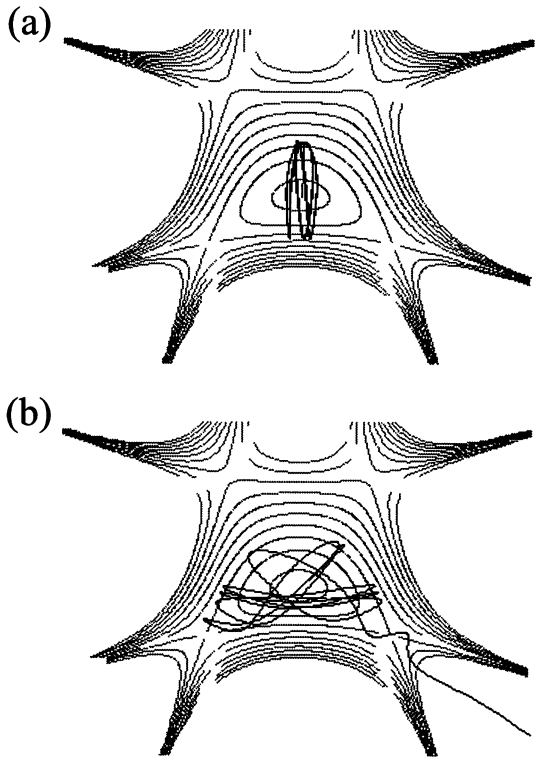

Figure 1. The q_1−q_2 dimensionless normal mode trajectories for the CS_2 molecule. The vertical axis is the q_1 coordinate, the horizontal axis is the q_2 coordinate. The antisymmetric coordinate q_3 is fixed at $\sqrt{2}$. The trajectories run with the same total energy E/hc = 1.2, but the initial conditions are $(q_1, q_2, q_3) = (6.60, 0.60, \sqrt{2})$ (a) and $(q_1, q_2, q_3) = (5.20, 3.58, \sqrt{2})$ (b). The initial kinetic energy is placed in the q_2 mode (i.e., initial $\dot{q}_1 = \dot{q}_3 = 0$)

Two examples of the trajectory plots are shown in Figure 1a,b. Both trajectories are calculated for a total energy of E/hc = 1.2, with different initial vibrational displacements of $(6.60, 0.60, \sqrt{2})$ and $(5.20, 3.58, \sqrt{2})$, respectively.

As shown in the trajectory plots, the trajectory in Figure 1a covers only a small part of the entire range of vibration modes, while the trajectory in Figure 1b covers a much broader range of q_1 and q_2. The implication of this difference is that a CS_2 molecule with E = 1.2, if starting from $(q_1, q_2, q_3) = (6.60, 0.60, \sqrt{2})$, will not dissociate even if the energy exceeds the dissociation energy, while a molecule with the same total energy, if starting from $(q_1, q_2, q_3) = (5.20, 3.58, \sqrt{2})$, will dissociate within a limited time.

A series of such calculations have been done at different total energies in order to demonstrate the effects of different initial normal mode coordinates on the dissociation rate. The dissociation rate was then plotted verses the q_2, q_1 normal coordinates. Some results are given in Figure 2 and Figure 3. Figure 2 plots the inverse of the dissociation time obtained by trajectory calculations versus the initial values of the q_1, q_2 dimensionless normal mode coordinates with total energy E/hc of 1.05, 1.10, 1.15, and 1.20, respectively.

Figure 3 is a plot of the inverse of the dissociation time obtained by trajectory calculations versus initial values of the q_1 dimensionless normal mode coordinates with different initial

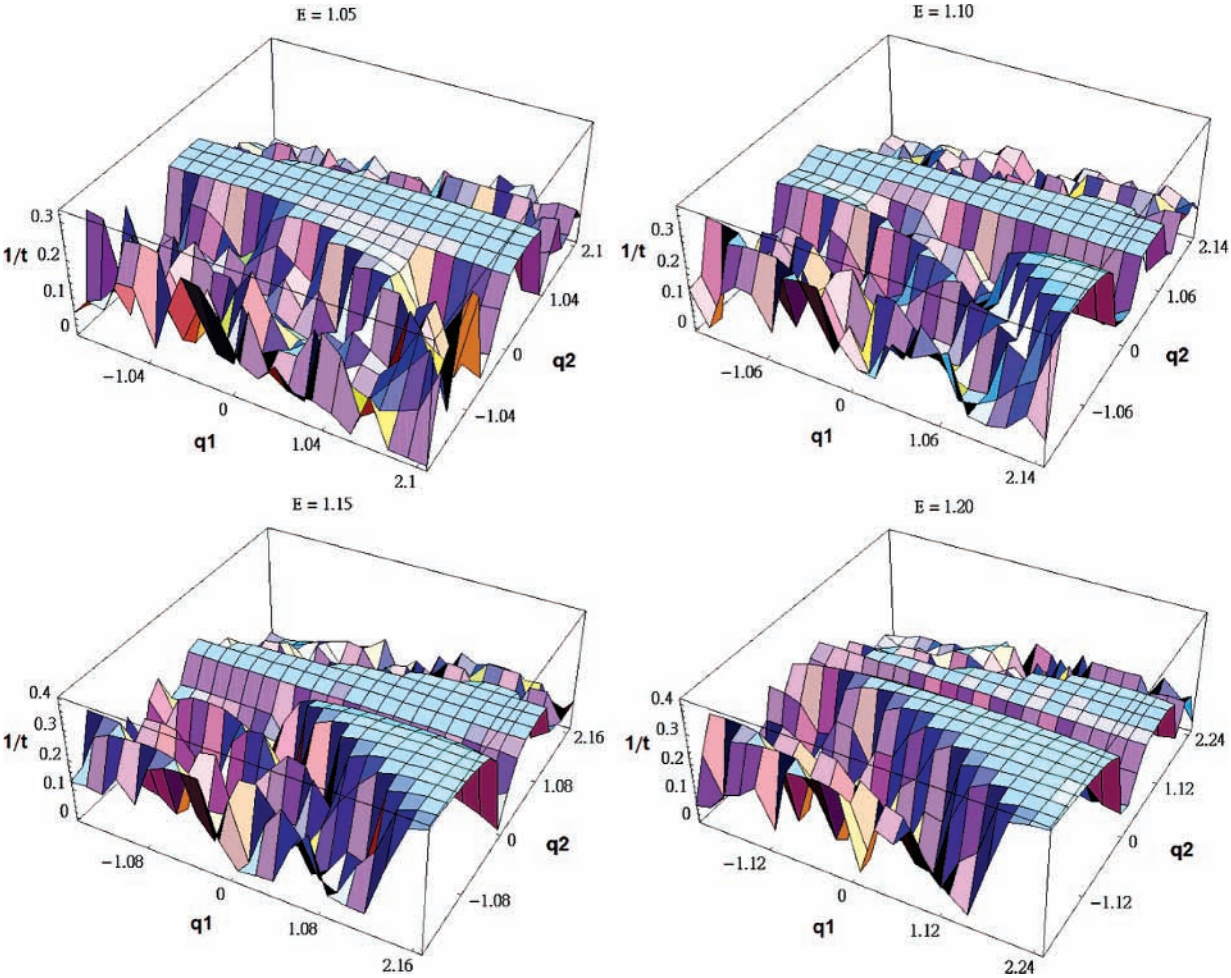

Figure 2. The inverse of the dissociation time obtained by trajectory calculations versus the initial values of the q_1, q_2 dimensionless normal mode coordinates. The antisymmetric coordinate q_3 is fixed at $\sqrt{2}$. The trajectory calculations for parts a−d were run with total energy E/hc fixed at 1.05, 1.10, 1.15, and 1.20, respectively.

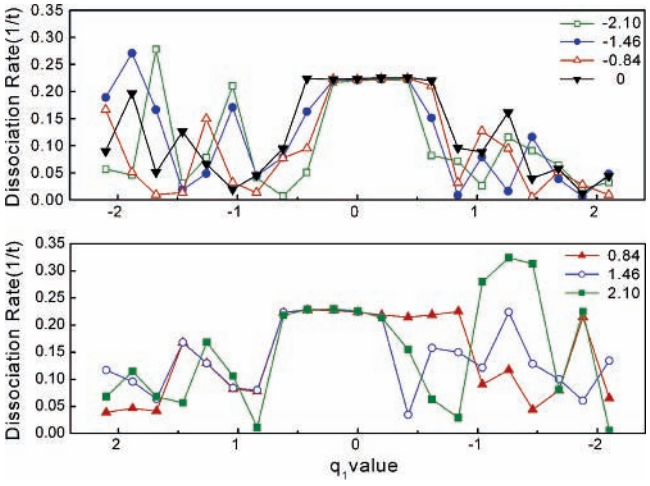

Figure 3. A plot of the inverse of the dissociation time obtained by trajectory calculations versus initial values of the q_1 dimensionless normal mode coordinate. The different lines represent different initial q_2 coordinates: empty squares represent initial q_2 at −0.105, solid circles represent initial q_2 at −0.073, etc. The total energy E/hc is 1.2 for this calculation.

q_2 coordinates from −2.1 to +2.1. The total energy E/hc is 1.2 for this plot.

As can be seen, for different total energies, that is E/hc = 1.05, 1.10, 1.15, and 1.20, respectively, from upper left to lower right in Figure 2, a distinct band is formed, where the dissociation rate is greatest.

When the total energy is near the energy of the saddle point on the potential energy surface ($E \sim 1$), the region with the highest dissociation rate is in the low vibration modes, that is to say, low initial values of q_1, q_2. As the excess energy becomes greater, the dissociation rate of the low q_2 vibration modes becomes increasingly lower, shown as the valley region in the plots below, and the dissociation rate at high vibration modes becomes greater. However, if instead of $p_2 = \mathrm{d}q_2/\mathrm{d}t = \sqrt{2}(E_0 - E_U)^{1/2}$we tak e$p_1 = \mathrm{d}q_1/\mathrm{d}t = \sqrt{2}(E_0 - E_U)^{1/2}$, $p_2 = 0$, and $q_2 = 0$ as the initial conditions, the trajectory will move along the vertical axis in Figure 1 and so does not result in dissociation.[17]

For the second series of calculations, we choose several points along several fixed potential energy contours [eq 4] on the ground-state surface of the CS_2 molecule as the initial dimensionless normal coordinates. The total energy E/hc is fixed for this calculation. The initial dimensionless normal coordinates are found by fixing the ratio of q_1 and q_2 ($\theta = \tan^{-1} q_1/q_2$; $0 \le \theta \le 2\pi$), then searching outward from the equilibrium point until the initial potential energy $V(q_1,q_2)$ equals a given value V_0. The initial kinetic energy E_{k0}, defined by the difference between the total energy E/hc and the initial potential energy $V(q_1,q_2)$, is placed in the q_2 normal mode (i.e., initial $\dot{q}_1 = \dot{q}_3 = 0$, $\dot{q}_2 = \sqrt{E/hc - V_0}$). The results are plotted in Figure 4.

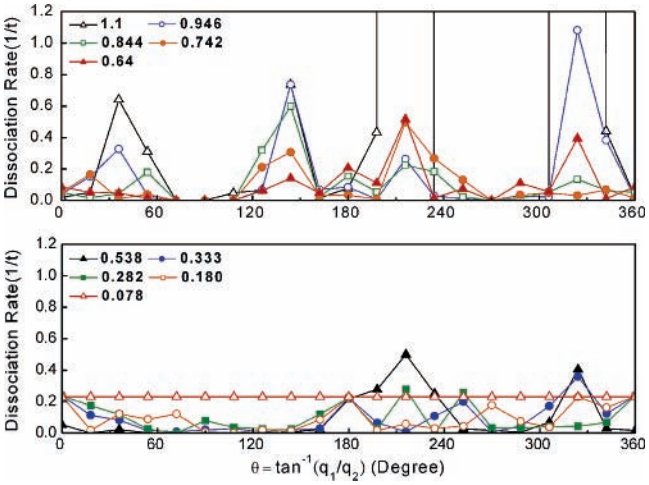

Figure 4. A plot of the inverse of the dissociation time obtained by trajectory calculations versus the arctangent of the initial ratio of the q_1 and q_2 dimensionless normal mode coordinates. The initial dimensionless normal mode coordinates are situated on fixed potential energy curves. The different lines represent different initial potential energy curves: empty squares correspond to an initial potential V of -0.844, solid circles represent an initial V of -0.333, etc. The total energy E/hc is 1.1 for this calculation.

Form these results it can be seen that for a classical trajectory calculation on a potential surface defined by eq 4, there are four directions, corresponding to the two saddle points and the two directions opposite to the saddle points, where the inverse of the dissociation time is greatest. The inverse of the dissociation time varies with the initial position, and is related to the shape of the potential surface. The initial potential energy determines the magnitude of the dissociation rate. The q_1, q_2 ratio that gives the highest dissociation rate for a given total and initial potential energy is determined by the shape of the potential energy surface.

C. Remarks. We have shown that in classical trajectory calculations, the rate of dissociation is highly dependent upon both the initial total energy and the initial amplitudes of the dimensionless normal modes of the molecule. Therefore, it is expected that if we prepare a real CS_2 molecule in highly excited vibration−rotation states, and then excite the molecule to dissociation energy, we will observe variations in the dissociation rate of the CS_2 molecule related to the initial vibration−rotation states.

III. Experiment

The concept of the experimental work is depicted in Figure 5.

The CS_2 molecule was chosen because (1) both the intermediate state (0 10 0) RB_2 and the highly vibrational states possess long lifetimes, which are suitable for population preparation by stimulated emission pumping, and (2) the spectroscopy is well studied. The rotationally resolved energy levels of each vibrational mode of the ground electronic state $X^1\Sigma_g^+$ of CS_2 from 3290 to 16370 cm^{-1} have been well studied by Liou et al. in 1998.[12] With this information, we are able to design an experiment that allows us to exactly excite the CS_2 molecule into any chosen vibrational mode of the ground electronic state by stimulated emission pumping (SEP) spectroscopy techniques. We can prepare a certain vibrational mode population to be the initial state and then excite the prepared molecules to a common predissociation band, Σ_0^g of the $^1B_2(^1\Sigma_u^+)$state, to begin dissociation. This has been reported previously by Liou et al. [12] using florescence as the detection scheme.

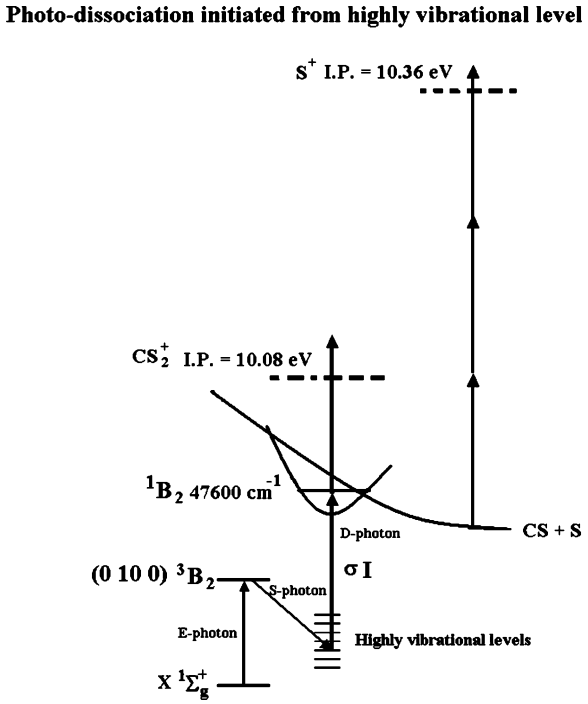

Figure 5. Energy diagram of CS_2 for $(1 + 1 + 1) + 1$ three-color multiphoton resonant ionization. The initial state population is prepared by stimulated emission pumping to a selected high vibrational state of the electronic ground state. The frequency of the third photon is scanned to excite the molecule to the predissociation state, then followed by absorption of another photon at the same frequency to ionize the parent molecule or fragments.

Our experimental setup using ion fragments as the detection scheme is depicted in Figure 6.

The experimental apparatus consists of three tunable dye-laser sources, a vacuum system, a molecular beam system, a TOF mass spectrometer, and a computer system for data acquisition. The laser system consists of one Nd:YAG laser (continuum PL 9030) system, from which the simultaneously lasing SHG (532 nm, 1.8 w) and THG (355 nm, 1.6 w) outputs were used to pump dye laser No. 1 (Lambda Physik FL 3002E) and Dye laser No. 2 (Lambda Physik FL 3002E), respectively. The laser dye Pyridine 1 was used for dye laser No. 1, and its output is red light (around 687 nm). This fundamental light was frequency doubled by a FL30 crystal to generate UV light (around 343 nm), denoted as the E-photon. The laser dyes Coumarin 102, 307, 153 and Rhodamine 6G were used for dye laser No. 2, with outputs ranging from 465 to 576 nm, denoted as the S-photon. The SHG lasing output (355 nm, 1.6 W) of another Nd:YAG laser (continuum NY-81-30) system was used to pump dye laser No. 3 (Lambda Physik FL 3002E). The dyes Coumarin 307 and 153 were used in dye laser No. 3 to generate fundamental light, with a range from 500 to 558 nm. This fundamental light was frequency doubled by a BBO1 crystal to generate UV output in the range from 250 to 279 nm. We denote this UV output of dye laser No. 3 as the D-photon.

The vacuum chamber consists of three major parts: source chamber, reaction chamber, and flight tube. A Blazer WKD 410 roots pump, connected to the source chamber, maintains the background pressure at 30 mTorr. A turbo pump of inlet diameter $\varphi = 8$ in. is connected to the reaction chamber to keep the pressure at 10^{-6} Torr throughout the experiment. Another turbo pump, inlet diameter $\varphi = 6$ in., is used to keep the flight tube at a pressure of 10^{-7} Torr. The sample we used is analytical grade CS_2 (99.9%) obtained from Fluka, and was used without further purification. CS_2 vapor at room temperature was allowed

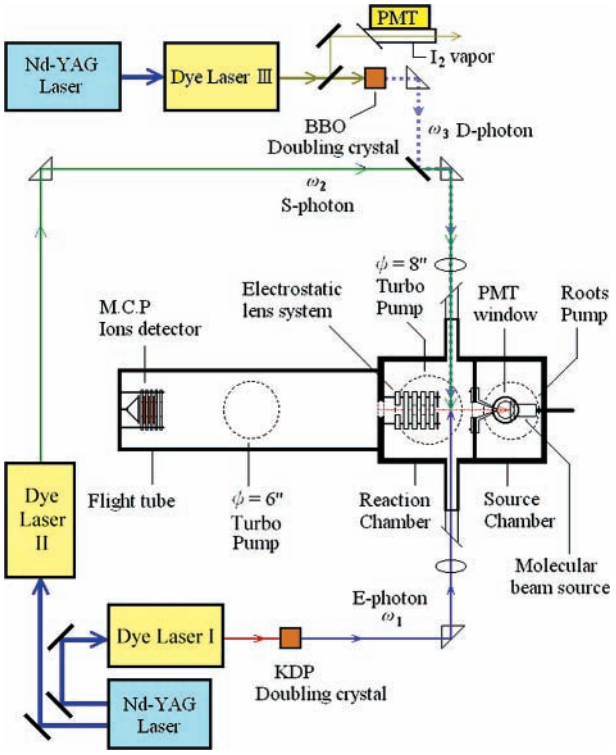

Figure 6. Schematic diagram of the experimental setup. Two fixed frequency YAG lasers were used to pump three tunable dye lasers. The output of Dye I was used to excite the molecules to the immediate state. The output of Dye II was used to carry out stimulated emission pumping to bring the molecule to the selected high vibrational state. The output of Dye III excites the molecule to the predissociation state, and ionizes the molecule and fragments as well. The ions were detected by a time-of-flight mass spectrometer.

to mix with a carrier gas of helium at 20 PSI, and then was expanded into the source chamber through a general valve (parker). The molecular beam is skimmed by a conical skimmer (diameter $\varphi = 1$ mm) before flying into the reaction chamber. The distance between the tip of the skimmer and the beam nozzle is 2.5 mm.

The E-photon and S-photon laser beams were introduced coaxially and counter-propagating, having both been focused by a 40 cm converging lens before entering the reaction chamber, with the S-photon delayed relative to the E-photon by 8 ns. The laser light beams are introduced through two Brewster windows, orientated so that the polarization of the light entering the reaction chamber is perpendicular to the molecular beam flight path (vertical polarization). The laser beams cross the molecular beam at the center of the chamber. The D-photon is propagated through the same path as the S-photon. Two synchronized pulse generators (DG 535, Stanford) are used to externally trigger the two Nd:YAG lasers. By adjusting the trigger time of each pulse generator, we set the D-photon to be delayed relative to the E-photon by 20 ns.

As shown in Figure 5, we used the E-photon to excite the CS_2 molecule up to a chosen rotational level (a chosen J level) of the (0 10 0) RB_2 state. Then we used the S-photon to transfer the CS_2 molecule down to one highly excited vibrational state of the electronic ground state via stimulated emission. Due to rotational selectivity, the S-photon can only transfer the molecule to the $\Delta J = 0, \pm 1$ rotational levels. Due to the symmetry of the CS_2 molecule, only the R-branch ($\Delta J = -1$) and P-branch ($\Delta J = +1$) transitions appear. In our experiment we select the $\Delta J = +1$, P-branch for study. By the above-mentioned SEP method, we can prepare the CS_2 molecule in one rotational level of any highly excited vibrational state of the electronic ground state, which we take to be the new initial state. By use of the D-photon, we excite the CS_2 molecule from the new initial state we have prepared to the energy level at 47562 cm^{-1}, i.e., to the Σ_0^g predissociation state, for further dissociation. We also diverted a fixed percentage of the fundamental light of dye laser No. 3 into I_2 vapor. An I_2 LIF spectrum was recorded simultaneously with each CS_2 ion spectrum to determine the real wavelength of the D-photon.

Behind the reaction chamber we set up a TOF (time-of-flight) mass spectrometer. The length of the flight tube is 90 cm with an MCP at the end to detect ions. In our experiment, four major ionic species, which can be identified as S^+, CS^+, S_2^+, and CS_2^+, were observed. The signal was fed into four boxcar integrators (Stanford Research SR 250) to monitor each resonant dip individually. The output from the boxcar integrator was then fed into an AD converter and interfaced to a PC for data storage.

Because all laser beams were focused by converging lenses, high photon intensities are present in the interaction region. The CS_2 molecule may thus absorb several E-photons or D-photons simultaneously to create ions. As an example, CS_2^+ can be generated by a CS_2 molecule absorbing three E-photons (343.8 nm, 3.61 eV), or by a CS_2 molecule absorbing three D-photons (279 nm, 4.45 eV), since both processes exceed the CS_2^+ ionization threshold energy of 10.08 eV. We denote this kind of ion generation as a one-color MPI (multiphoton ionization) process. These one-color MPI ions form a part of the background noise for our experiment. The energy of the S-photon, which ranges from 2.16 to 2.7 eV, is much lower than that of the E-photon and D-photon, and so is unlikely to cause one-color MPI processes. Also, Liou et al. in 1997[13] have reported that converged and highly intense S-photons can excite a CS_2 molecule from the (0 10 0) RB_2 state up to both a repulsive dissociation state and the $^1B_2(\Sigma_u^{1+})$ predissociation state, which goes against our original expectation for the S-photon. Therefore, the intensity of all three laser beams must not be overly intense, yet must also not be so weak as to be unable to generate sufficient ionization. The intensity of each beam must be maintained at a suitable level. Experimentally, we find that the optimal conditions are to hold the intensity of the E-photon at around 3 mJ, the intensity of the S-photon at around 1.8 mJ, and the intensity of the D-photon at around 2 mJ. Under such conditions, one-color ionization becomes insignificant, yet E-photon and D-photon two-color ionization is still sufficiently strong.

In our experiment we monitor S^+, CS^+, S_2^+, and CS_2^+ ions simultaneously, while scanning the wavelength of the D-photon. Resonance structure in the spectra was observed for the CS_2^+ and S^+ ion signals. The resonance structure is due to REMPI (resonance enhanced multiphoton ionization) processes. We did not observe resonance structure for the CS^+ and S_2^+ ion signals corresponding to the CS_2^+ and S^+ ion signals.

In this experiment, we selected a total of 16 vibrational states, from (0 18 0) up to (1 26 0), on the electronic ground state of CS_2 to prepare as initial states. In the (0 22 0) level we selected rotational levels with $J_2 = 24, 28, 30, 32$. In the others we selected rotational levels with $J_2 = 18, 22, 24, 28$ for our study. The observed spectral lines were numerically fit to a Lorenzian line profile by analysis software (PeakFit) to determine the central transition frequency and fwhm of each transition line. The dissociation rate of CS_2 was determined from the uncertainty relationship $\Delta T = \hbar/\Delta E$.

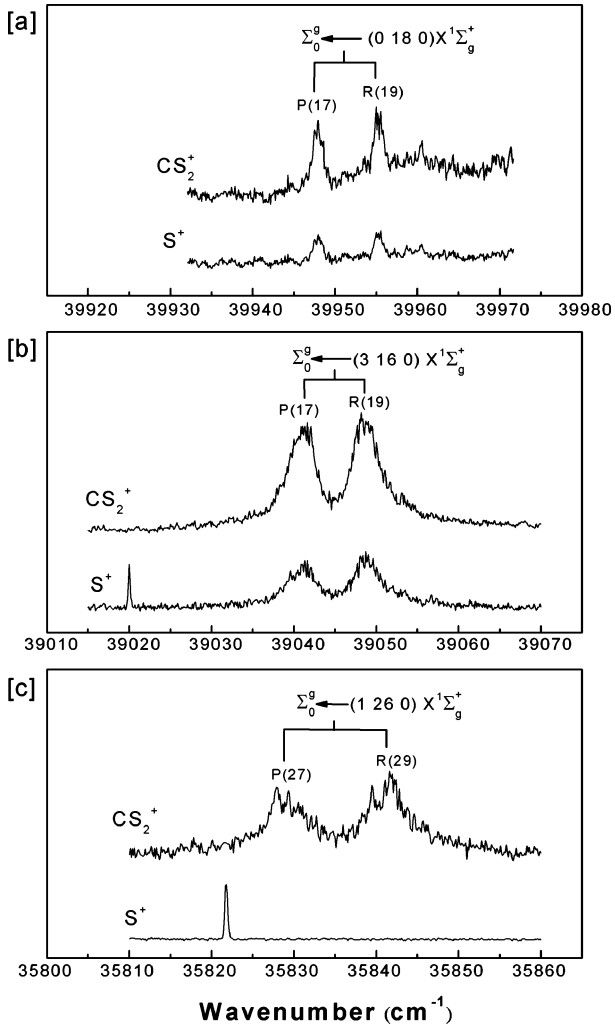

Figure 7. REMPI spectra of CS_2 which were initiated from three highly excited vibrational states of the electronic ground state (a) (0 18 0), (b) (3 16 0), (c) (1 26 0), and which terminated in the same Σ_0^g predissociation state.

IV. Results and Discussion

Figure 7 shows three $(1 + 1 + 1) + 1$ resonant multiphoton ionization rotationally resolved spectra taken under the time-of-flight mass-spectrometry scheme. The first transition, with a fixed frequency, is to the intermediate electronically excited (0 10 0) RB_2 state. The second transition, with a fixed frequency, is to the selected highly excited vibrational state of the $X^1\Sigma_g^+$ electronic ground state. The frequency of the third photon was scanned over the predissociating vibrational state Σ_0^g of $^1B_2(\Sigma_u^{1+})$, where the dissociation occurs. The fourth transition, with the same frequency as the third photon, ionizes the parent molecule or the dissociation fragments. Both CS_2^+ and S^+ ions are detected as the wavelength is scanned. The two transition peaks in each spectrum correspond to one P and one R branch line, respectively. The spectrum is rotationally resolved because only one particular J level of each vibrational state was populated by SEP preparation. Figure 7a is the spectrum that the third photon transition initiates from $J = 18$ of the (0 18 0) vibration mode. The transition line width fwhm is 1.2 ± 0.2 cm^{-1}. Figure 7b is the spectrum that the third photon initiates from $J = 18$ of the (3 16 0) vibration mode. The transition line width fwhm is 5.5 ± 1 cm^{-1}. The line width is partly due to power broadening. Figure 7c is the spectrum that the third photon transition initiates from $J = 18$ of the (1 26 0) vibration mode. The transition line width fwhm is 7 ± 1 cm^{-1}. The line width is again partly due to power broadening. It is of particular interest that in Figure 7c only the CS_2^+ ion was detected. This implies that dissociation is slower than ionization. The spectra in Figure 7 clearly show that different initial states result in different transition line widths and dissociation mechanisms, even though the transitions end at the same final state. Both power broadening and predissociative lifetime broadening contribute to the transition line width. Figure 8 shows that the line width of the initial state in Figure 7 increases with laser intensity. This increase in line width is due to the power broadening of the transitions.

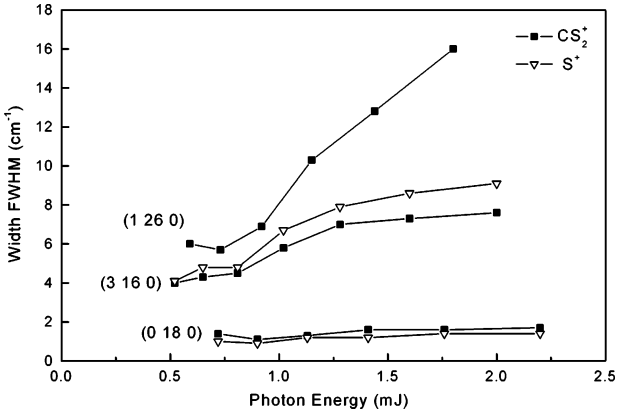

Figure 8. Predissociation line widths in CS_2 caused by photoexcitation to Σ_0^g from the high vibrational states (1 26 0), (3 16 0), and (0 18 0) of the electronic ground state versus the intensity of the dissociation photon. The ■ curve and the ▽ curve represent CS_2^+ and S^+ ions, respectively, which were monitored in a wavelength scanned mass spectrometer. Note that for (1 26 0) the signal of the S^+ ion was too weak to be compared with that of the CS_2^+ ion.

For (3 16 0) and (1 26 0), power broadening was clearly observed, while power broadening for (0 18 0) is insignificant. The power broadening of each initial vibrational state could be due to Franck−Condon factors that result in transition strengths strong enough to cause the power broadening. Because the lowest electronically excited state, RB_2, is far above those vibrational states of the electronic ground state, and no decay mechanism has been reported, the lifetime broadening of those initial vibrational states has an insignificant contribution. The line width, power broadening excluded, can be regarded as a lifetime broadening caused by predissociation. As indicated in Figure 8, some initial states result in power broadening, some do not. The power broadening being due to the transition strength and the lifetime broadening being due to the predissociation, they cannot be distinguished because both processes give the same Lorentzian line profile. However, one could find a minimum value of lifetime broadening from those initial states which do not show power broadening. Among the observed states, the smallest line width is found for (0 22 0), with band origin at 9367.63 cm^{-1}, and the power broadening of this state is insignificant. It is reasonable to assume that this is the smallest predissociation line width. For those initial states processing power broadening, the line widths shown in Figure 8 were deduced by extrapolating to a D-photon intensity of 0.2 mJ. The value 0.2 mJ was chosen to ensure that the line width of all those broadening states at this photon intensity is greater than the minimum line width. Figure 9 shows how the deduced line widths, i.e., line widths at photon intensity 0.2 mJ, vary for various initial vibrational states. Even though power broadening cannot be completely ruled out, Figure 9 is able to

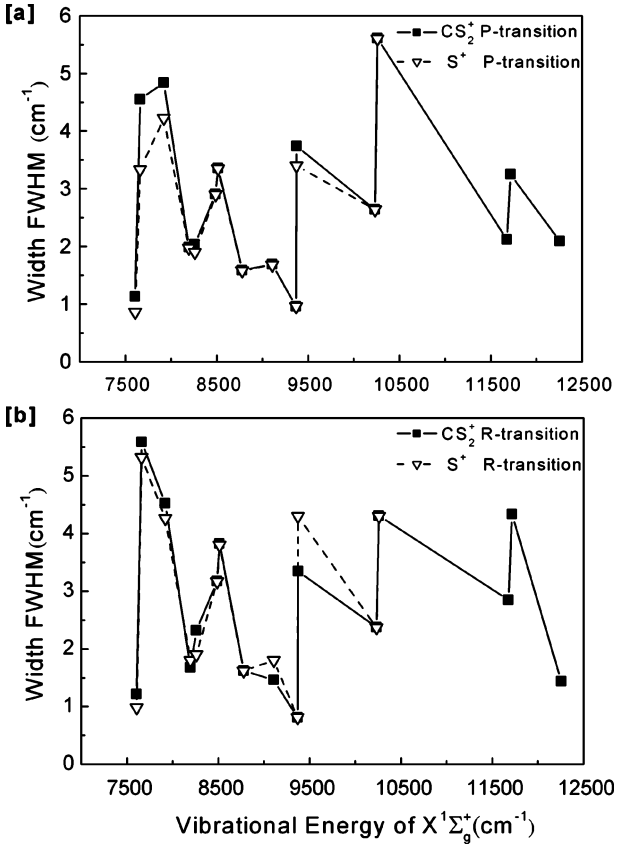

Figure 9. Predissociation line widths in CS_2 caused by photoexcitation to Σ_0^g from high vibrational states of the electronic ground state at various energies. The line width is taken at weak photon intensity where the broadening effect is a minimum. Line widths of both P-transitions and R-transitions are plotted. The ■ curve and ▽ curve represent CS_2^+ and S^+ ions, respectively, which were monitored in a wavelength scanned mass spectrometer.

qualitatively show the lifetime broadening variation with initial state at certain energies.

V. Conclusion

According to the Franck−Condon principle, the motion of the nuclei in a photodissociation process starts from coordinates possessing the potential energy of the initial state. It is of interest to know whether during the dissociation, the motion of nuclei will be governed by the potential surface of the initial state or final state. The result of trajectory calculations shows that given a total energy greater than the dissociation, the dissociation rate varies with the initial conditions such as coordinates, kinetic energy, and potential energy. And the dissociation rate is mode dependent. The experimental results show that the line width caused by the predissociation varies with initial state. These results show that the predissociation rate depends on the initial state. It provides a possibility to manipulate a photochemical reaction by selecting the initial state.

Acknowledgment. The authors wish to thank Dr. Kuang Lang Huang for his previous work. Huei Tarng Liou wishes to thank Dr. John Hougen for his help and AirTree Ozone Technology for the financial support of this study.

References and Notes

(1) Harringtom, R. E.; Rabinovitch, B. S.; Frey, H. M. *J. Chem. Phys.* **1960**, *33*, 1271.
(2) Hardwidge, E. A.; Rabinovitch, B. S.; Ireton, R. C. *J. Chem. Phys.* **1973**, *58*, 340.
(3) Sture, K.; Nordholm, J.; Rice, S. A. *J. Chem. Phys.* **1974**, *60* (1), 203.
(4) Uzer, T.; Hynes, J. T.; Rienhardt, W. P. *Chem. Phys. Lett.* **1985**, *117* (6), 600.
(5) Baer, T.; Hase, W. L. *Unimolecular Reaction Dynamics*; Oxford University Press: Oxford, UK, 1996.
(6) Frost, W. *Theory of Unimolecular Reactions*; Academic Press: New York, 1973.
(7) Atkins, P. W.; Friedman, R. S. *Molecular Quantum Mechanics*; Oxford University Press: Oxford, UK, 1997.
(8) Wolf, R. J.; Hase, W. L. *J. Chem. Phys.* **1980**, *73* (8), 3779.
(9) Nielsen, H. H. *Rev. Mod. Phys.* **1951**, *23*, 90.
(10) Kuchitsu, K.; Morino, Y. *Bull. Chem. Soc. Jpn.* **1965**, *38* (3), 805.
(11) Suzuki, I. *Bull. Chem. Soc. Jpn.* **1975**, *48* (6), 1685.
(12) Liou, H. T.; Huang, K. L. *Chem. Phys.* **1999**, *246*, 391.
(13) Nielsen, A. H. *J. Chem. Phys.* **1943**, *11*, 160.
(14) Pique, J. P. *J. Opt. Soc. Am. B* **1990**, *7*, 1816.
(15) Press, W. H., et al. *Numerical Recipes*; Cambridge University Press: Cambridge, UK, 1986.
(16) Hase, et al. *Advances in Classical Trajectory Methods*; Jai Press Inc.: London, UK, 1992.
(17) Slater, B N. *Theory of Unimolecular Reactions*; Cornell University Press: Ithaca, NY, 1959.
(18) Liou, H. T.; Chang, Y. C.; Huang, K. L.; Lin, W. C. *J. Phys. Chem. A* **1997**, *101*, 6723.
(19) McCrary, V. R.; Lu, R.; Zakheium, D.; Russell, J. A.; Halpern, J. B.; Jackson, W. M. *J. Chem. Phys.* **1985**, *83* (7), 3481.
(20) Waller, I. M.; Hepburn, J. W. *J. Chem. Phys.* **1987**, *87* (6), 3261.
(21) Tzeng, W. B.; Yin, H. M.; Leung, W. Y.; Luo, J. Y.; Nourbakhsh, S.; Flesch, G. D.; Ng, C. Y. *J. Chem. Phys.* **1988**, *88* (3), 1658.